

Trading spaces: building three-dimensional nets from two-dimensional tilings

Toen Castle, Myfanwy E. Evans, Stephen T. Hyde, Stuart Ramsden and Vanessa Robins

Interface Focus published online 25 January 2012
doi: 10.1098/rsfs.2011.0115

References

[This article cites 21 articles](#)

<http://rsfs.royalsocietypublishing.org/content/early/2012/01/24/rsfs.2011.0115.full.html#ref-list-1>

P<P

Published online 25 January 2012 in advance of the print journal.

Subject collections

Articles on similar topics can be found in the following collections

[biocomplexity](#) (13 articles)

Email alerting service

Receive free email alerts when new articles cite this article - sign up in the box at the top right-hand corner of the article or click [here](#)

Advance online articles have been peer reviewed and accepted for publication but have not yet appeared in the paper journal (edited, typeset versions may be posted when available prior to final publication). Advance online articles are citable and establish publication priority; they are indexed by PubMed from initial publication. Citations to Advance online articles must include the digital object identifier (DOIs) and date of initial publication.

To subscribe to *Interface Focus* go to: <http://rsfs.royalsocietypublishing.org/subscriptions>

Trading spaces: building three-dimensional nets from two-dimensional tilings

Toen Castle, Myfanwy E. Evans, Stephen T. Hyde*,
Stuart Ramsden and Vanessa Robins

*Department of Applied Mathematics, Research School of Physics and Engineering,
The Australian National University, Canberra, Australian Capital Territory 0200, Australia*

We construct some examples of finite and infinite crystalline three-dimensional nets derived from symmetric reticulations of homogeneous two-dimensional spaces: elliptic (S^2), Euclidean (E^2) and hyperbolic (H^2) space. Those reticulations are edges and vertices of simple spherical, planar and hyperbolic tilings. We show that various projections of the simplest symmetric tilings of those spaces into three-dimensional Euclidean space lead to topologically and geometrically complex patterns, including multiple interwoven nets and tangled nets that are otherwise difficult to generate *ab initio* in three dimensions.

Keywords: two-dimensional nets; three-dimensional tiling; symmetry

1. INTRODUCTION

This paper surveys three-dimensional net-like structures derived from symmetric reticulations of two-dimensional surfaces. Our focus is on the arrangements of edges and vertices in intersection-free tiled surfaces, or polyhedra, which can assume surprisingly convoluted arrangements. We consider polyhedra that are unions of contiguous, non-overlapping faces, made up of vertices and edges. Both edges and faces are free to curve and the polygons comprising faces can be infinite. The examples resulting from this more liberal definition of polyhedra—beyond the more common view of polyhedra as plane-faced convex solids—are remarkably rich in variety, despite our focus on polyhedra as tiled surfaces rather than volumes.

Given the endless possible shapes of tilings, it is useful to group them into manageable sets, called *equivariant tilings*, that conflate all tilings which share common symmetry and topology into a single class. We describe symmetry using the concept of orbifolds, and topology with Schläfli symbols, both introduced in the next section. Thanks to the advances in combinatorial tiling theory owing to Dress [1], Huson [2] and Delgado-Friedrichs [3], systematic enumeration of equivariant classes of tilings is feasible up to an arbitrary degree of complexity for all two-dimensional geometries.

Our goal is to construct nets—patterns of edges in three-dimensional Euclidean space (E^3). We approach E^3 via a circuitous path that allows us to remain in two-dimensional space, and enumerate two-dimensional

nets as edges of two-dimensional tilings; a task that is considerably simpler than three-dimensional constructions. Once this construction is in place, these two-dimensional structures are mapped into three-dimensional nets as a final step. That relies on the embedding of the two-dimensional manifold that is reticulated by the two-dimensional tiling. We shall see that although we choose only the simplest embeddings of relevant surfaces, the resulting three-dimensional nets can have very complex structures, more complex than could have been systematically generated *ab initio* in three dimensions.

We look first at the most symmetric polyhedra that emerge from tilings of the sphere (S^2), then explore generalized polyhedral forms that result from tilings of the Euclidean (E^2) and hyperbolic planes (H^2).

2. TILINGS OF S^2 : PLATONIC POLYHEDRA

The beauty of simpler symmetric convex polyhedra has surely been appreciated for millenia. The most regular polyhedra with flat faces and rectilinear edges—the tetrahedron, cube, octahedron, dodecahedron and icosahedron—are described in Plato's *Republic* [4]. Proof that these polyhedral Platonic solids exhaust the list of regular polyhedra is perhaps the simplest illustration of the power of accessing three-dimensional space via a two-dimensional surface.

A convex polyhedron can be ‘inflated’, so that its faces are all equally curved and lie on a sphere, which is the simpler non-Euclidean space in two dimensions (S^2). This process is illustrated for the cube in figure 1. Each face is now a spherical polygon, bounded by edges that are portions of great circles on S^2 (i.e. geodesics). Such a pattern is a *tiling* of the sphere; it

*Author for correspondence (stephen.hyde@anu.edu.au).

One contribution to a Theme Issue ‘Geometry of interfaces: topological complexity in biology and materials’.

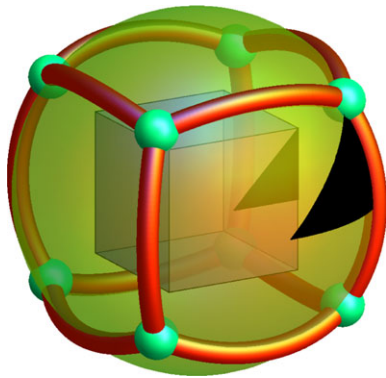


Figure 1. Projection of a cube onto a sphere, so that all faces become spherical polygons bounded by great-circular edges. This defines a tiling of the sphere. A single ‘flag’ of the tiling is marked (black triangle).

is characterized by non-overlapping tiles that meet edge-to-edge and cover the entire surface.

The *topology* of two-dimensional tilings is captured by integers that measure (i) the number of edges around each tile (polygon size) and (ii) the number of tiles sharing a common vertex. A honeycomb tiling, for example, as in figure 3*a*, is composed of hexagonal tiles and has *Schläfli symbol* $\{6,3\}$, since the values of indices (i) and (ii) are identical for all tiles and vertices. Figure 1 shows that the tiling of S^2 derived from the cube has *Schläfli symbol* $\{4,3\}$.

Platonic polyhedra are very symmetric in three-dimensional space. The vertices, edges and faces are *transitive*: they are mapped into each other by reflections in the suite of mirror planes that intersect at the polyhedral centres. These symmetries define the point groups. The corresponding two-dimensional symmetries are generated by reflections along mirror lines that lie along edges of elementary triangles called flags. A *flag* of a two-dimensional tiling has one point on a vertex of the tiling, a second on the mid-point of an adjacent edge and a third point at the centre of an adjacent tile.

The Platonic tilings with *Schläfli symbol* $\{n,z\}$ have only a single flag type: a spherical triangle whose geodesic arcs meet at $\pi/2, \pi/n, \pi/z$. An elementary theorem of spherical geometry relates the area of a triangle A_δ on a sphere of radius r to the sum of its vertex angles

$$A_\delta = \left(\frac{1}{2} + \frac{1}{n} + \frac{1}{z} - 1 \right) \pi r^2 \quad (2.1)$$

and we know the total surface area of a sphere is $4\pi r^2$.

Since the flags of a Platonic polyhedron tile the sphere once, we can derive a condition for the number of flags, N_δ :

$$N_\delta = \frac{8nz}{2(n+z) - nz}. \quad (2.2)$$

These equations allow the enumeration of the Platonic polyhedra as flag-transitive tilings of S^2 . Integer solutions of equation (2.2) are listed in table 1. Solutions with $n > 2$ can be embedded in E^3 as the five Platonic polyhedra, whose point groups symmetries have orders 24, 48, 120, 48 and 120, respectively (i.e. N_δ). So Plato’s list exhausts all plane-faced

Table 1. Flag-transitive tilings of S^2 , with *Schläfli symbol* $\{n,z\}$ and N_δ flags.

$\{n,z\}$	N_δ	polyhedron
$\{2,k\}$	$4k$	‘lunar’ polyhedra
$\{3,3\}$	24	tetrahedron
$\{3,4\}$	48	octahedron
$\{3,5\}$	120	icosahedron
$\{4,3\}$	48	cube
$\{5,3\}$	120	dodecahedron

convex regular polyhedra, but an infinite number of ‘lunar’ polyhedra, necessarily containing curved edges and faces, are similarly regular.

3. ORBIFOLDS

The Platonic polyhedra can be viewed as *kaleidoscopic* tilings of S^2 : in each case, the flags are bounded by mirror lines. There are a number of different systems for describing and naming two-dimensional symmetry groups. We adopt the language of *orbifolds* [5,6], as it affords a unified notation system for all three two-dimensional spaces of constant curvature. For our purposes, an orbifold is the two-dimensional asymmetric domain of a pattern in the relevant space (S^2 , H^2 or E^2). The kaleidoscopic regular tilings of S^2 , for example, have symmetry $*2nz$. Here, the asterisk (*) denotes a mirror boundary, with 2, n and z mirror lines intersecting at the flag vertices. We call all such orbifolds bounded entirely by mirror lines *Coxeter orbifolds*; their symbols are of the form $*ijk\dots$, where i, j , etc. are integers necessarily greater than 1. Allowed Coxeter orbifolds in S^2 are rather limited: $*jj$, $*22j$ and $*23k$, where $j \in \{2, 3, \dots\}$ and $k \in \{3, 4, 5\}$. It is important to note that these orbifolds act on the two-dimensional surface of the sphere S^2 only. Embedding the sphere in three-space allows translation of these two-dimensional symmetries to the usual point group notations ($*jj$ translates to Schoenflies symbols C_{jv} ; $*22j$ are equivalent to D_{jh} and $*23k$ are equivalent to the Schoenflies names T_d , O_h and I_h when $k = 3, 4, 5$, respectively).

Other orbifolds are possible in S^2 , and lift to the usual point groups. Here, we mention just two further classes of orbifolds, *stellate* and *hat* orbifolds. These names come from the shape of these orbifolds, which resemble stellated spheres and generic, occasionally multi-pointed, hats (with a single bounding edge, to sit on the wearer’s head). Stellate examples are characterized by the presence of rotational symmetries only. So, for example, the chiral point groups I , O and T result from embeddings in three-space of patterns on S^2 with orbifolds 235, 234 and 233, respectively. Stellate orbifolds have symbols of the form $IJK\dots$, where the integers I , etc. denote the order of rotational symmetry. Hat orbifolds combine rotations (not on mirror lines) with mirror boundaries, and have the generic symbol $IJK\dots*ijk\dots$. For example, the three-dimensional point groups D_{jd} arise from orbifolds of types $2*j$, while those with Schoenflies symbol C_{Kh} emerge from

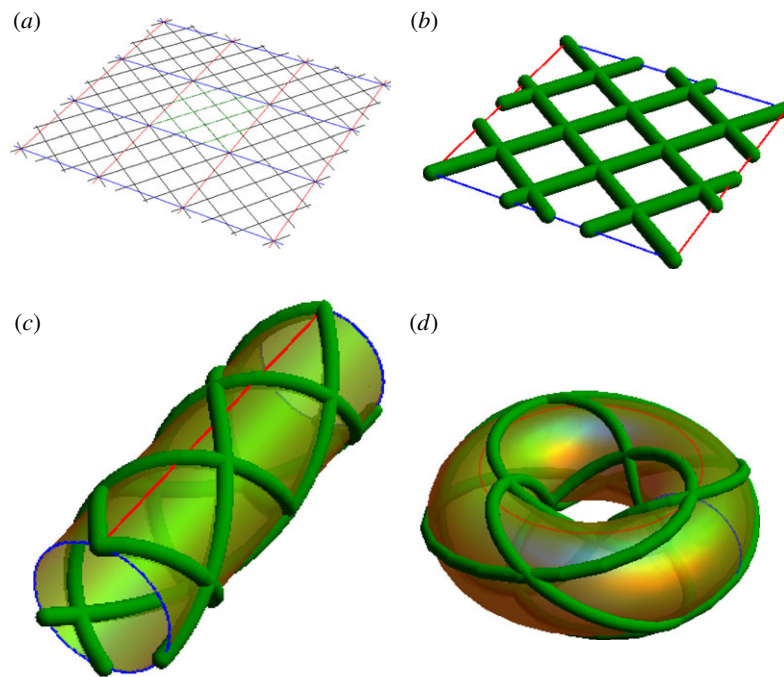


Figure 2. (a) The two-periodic $\{4,4\}$ net in E^2 , with arbitrary unit cells delineated by blue and red lines. (b) Excision of a single unit cell. (c) If all points separated by one of the lattice vectors are identified with each other, a one-periodic reticulation of a cylinder results. (d) A toroidal reticulation is formed if all points separated by the second lattice vector are also glued.

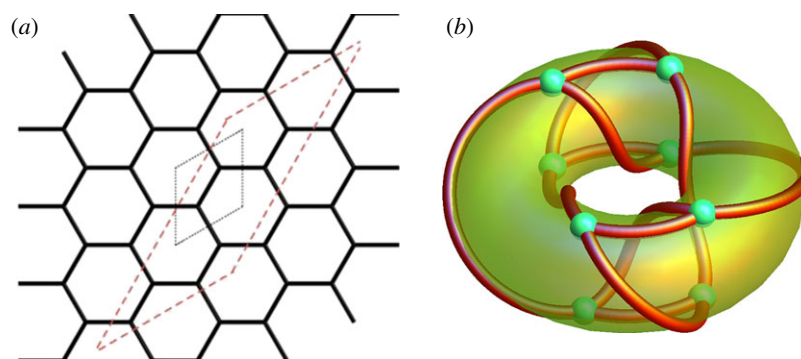


Figure 3. (a) The two-periodic $\{6,3\}$ net in E^2 with primitive lattice vectors \mathbf{a} and \mathbf{b} (full grey lines) can be wrapped onto a torus using the vectors $2\mathbf{a}$ and $2\mathbf{a} + 2\mathbf{b}$ (dashed lines). (b) The resulting $\{6,3\}$ reticulation of the torus.

three-space embeddings of patterns on S^2 whose orbifolds are of the form K^* .

4. TWO-PERIODIC TILINGS OF E^2

Consider next tilings of the Euclidean plane, E^2 . We restrict our attention to *two-periodic* examples that contain a pair of translations as a subgroup. Allowed symmetries are the 17 plane groups, well-known to crystallographers. All of these symmetries can be generated from ‘flat’ orbifolds, which include Coxeter, stellate and hat examples: e.g. $*236$ (or, in the nomenclature of plane groups, $p6mm$), 244 ($p4$) and 2^*22 (cm) respectively.

S^2 can only be embedded in three-dimensional space in one way: the two-dimensional sphere. In contrast, there are many simple embeddings of E^2 into three-dimensional space. The simplest is the usual embedding of the plane in E^3 , extending without limit in two independent directions (figure 2a). Alternatively, one or

both of the two translations can be factored out, by wrapping the plane an infinite number of times around a cylinder or a torus. These cases give planar, cylindrical and toroidal polyhedra.

A cylindrical polyhedron can be constructed by mapping a lattice vector to an equatorial line of the cylinder, as illustrated in figure 2b,c. However, any lattice vector can be mapped to an equator of the cylinder, giving both chiral and achiral examples of reticulated cylinders with various radii. This construction is reminiscent of that used to describe carbon nanotubes in terms of the planar graphene ($\{6,3\}$) lattice [7]. Note that only a single lattice vector has been ‘lost’ by cylinder formation; so these cylindrical tilings are one-periodic in three-dimensional space.

The remaining lattice vector can also be used to map the cylinder back onto itself, to generate a tiling of the donut-like *torus*, shown in figure 2d—a toroidal polyhedron. This construction deserves deeper scrutiny, as it exemplifies some of the subtleties

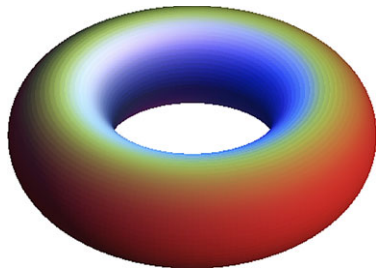


Figure 4. Embedding of the Euclidean torus in E^3 , coloured by the curvature distortions induced by the embedding. The curvature ranges from negative (blue) to positive (red), though it is on average zero (yellow).

of embedding two-dimensional patterns in three-dimensional space.

4.1. Toroidal nets

First, the abstract two-dimensional space formed by identifying all points in E^2 separated by a pair of lattice vectors (\mathbf{a} and \mathbf{b}) is flat (Euclidean), since it inherits exactly the same metric structure as the plane itself. That is not true, however, for the torus embedded in E^3 . The torus is saddle-shaped (and hyperbolic) in the vicinity of the inner hole, but bowl-shaped (elliptic) on the outer regions making it on average flat, but with significant variations of curvature (figure 4).

Second, any pair of independent lattice vectors ($i\mathbf{a} + j\mathbf{b}$ and $k\mathbf{a} + l\mathbf{b}$, say, where i and j are integers) can be used to form a toroidal tiling from the single $\{6,3\}$ tiling of E^2 ; choosing different pairs gives toroidal tilings of distinct winding character on the torus. The area of the parallelogram determines the number of distinct vertices in the resulting toroidal net. For example, the $\{6,3\}$ net, with two vertices per unit cell and \mathbf{a} and \mathbf{b} as shown in figure 3, forms a toroidal net with $2(il - jk)$ vertices in the torus.

The example in figure 3 uses vectors $2\mathbf{a}$ and $2\mathbf{a} + 2\mathbf{b}$ and has eight vertices. More complex examples, formed by gluing the lattice vectors $4\mathbf{a}$ and $2\mathbf{a} + \mathbf{b}$, are shown in figure 5. These too have eight vertices and differ only in the gluing locations relative to the embedded torus. Seams can be on either the inner or outer equators of the torus and the gluing order is flexible, allowing the construction of ‘inside-out’ versions of toroidal nets.

4.2. Net isotopes

Remarkably, *all* of the toroidal nets in figures 3 and 5 are topologically equivalent as graphs—they have the same underlying combinatorial structure. For example, they each contain eight vertices of degree-3 and six fundamental cycles, each of length four. Comparison of projections of these toroidal cubes with that of the normal cube (figure 6) lays bare their common topologies. However, the nets are embedded in E^3 differently and cannot be deformed from one to the other without cutting edges. Evidently, the conventional embedding (figure 1) is untangled and the examples of figures 3

and 5 are tangled. We therefore need some method to recognize distinct *entanglements* of these cube graphs.

The question of tangled nets is a very complex one that remains largely unexplored. A simpler phenomenon—better explored mathematically—is knots. A mathematical knot, though tangled, is topologically equivalent to a simple loop (S^1). Equivalent knots are *ambient isotopic*; i.e. they can be deformed into each other without cutting and retying. We call two embedded (possibly tangled) nets that can be morphed into each other via ambient isotopy *isotopes*. A major concern of knot theory is the question of when two embeddings of S^1 represent equivalent knots, i.e. whether they are ambient isotopic. Even this problem is still not completely resolved; the analogous question for tangled graphs—namely to decide if two nets are equivalent or distinct isotopes—is even more complex. One approach is to examine the set of knots and links generated by all cycles in the net, leading to the invariants of Kauffman [8]. Two nets with the same graph structure and distinct knots and links must be distinct isotopes, so Kauffman’s invariants that afford necessary conditions for two embeddings to be distinct isotopes. This approach proves that the cube isotopes illustrated in figures 1, 3 and 5 are distinct isotopes of the cube graph.

An alternative numerical approach to Kauffman’s invariants is under development, which, if sufficiently convergent and accurate, offers a strictly geometric, though numerical, route to answering whether nets are distinct isotopes. The idea is adapted from the *SONO algorithm* [9], developed to give canonical, or ‘tight’, embeddings of knots in E^3 , starting from any given embedding. The knot is modelled by an infinitely flexible and frictionless rope of a given diameter (D), and the rope is forbidden to intersect itself (i.e. points in nearby sections of the knot trajectory must not be closer than D units). The energy of the knot conformation is gauged by the ratio of rope length to diameter, which is minimized for the tight embedding.

The SONO algorithm has been extended to admit tight embeddings of finite and periodic graphs [10]. It has been tested on a number of examples with success, affording a numerical estimate of a ‘canonical’ embedding of net isotopes. For example, tight embeddings of the toroidal cube isotopes shown in figures 3 and 5 are shown in figure 7. These are very different geometrically, as expected for different isotopes, which supports the notion of finding a canonical embedding for isotopes. In general, however, global minimizers of the modified SONO energy may not be geometrically unique [10].

Enumeration of tangled versions of polyhedral nets via two-periodic tilings of E^2 is possible using the above approach. We will publish elsewhere a systematic derivation of toroidal nets that are topologically equivalent to the net of edges of the simpler Platonic polyhedra, namely the tetrahedron, octahedron and cube [11]. An earlier partial enumeration of tangled cubes offers an introduction to this approach [12]. These toroidal examples represent the simplest examples of tangled polyhedral nets; more complex

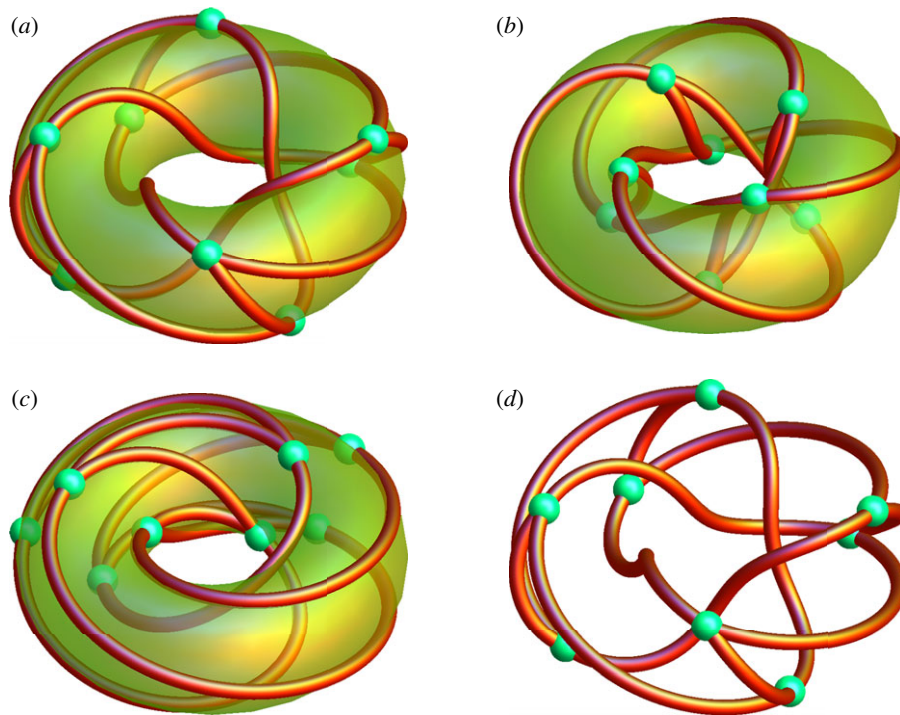


Figure 5. A more oblique pair of lattice vectors than those of figure 3 generates more highly wound nets. All four embeddings shown here are generated by gluing vectors $4\mathbf{a}$ and $2\mathbf{a} + \mathbf{b}$. They differ only in the position of the seams of the gluing on the torus: (a) has $4\mathbf{a}$ running along the inner equatorial line, (b) along the outer equatorial line, while (c) has $2\mathbf{a} + \mathbf{b}$ mapped to the equator. (d) The net embedding in space formed by the toroidal tiling of (a).

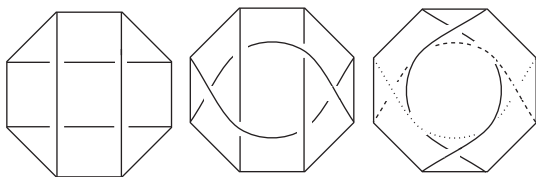


Figure 6. Projections of the cube isotopes in figures 1, 3 and 5 respectively.

cases can be deduced by extending this process to reticulations of two-dimensional surfaces of higher genus.

An important characteristic of toroidal entanglements of polyhedra whose untangled forms reticulate S^2 is the emergence of *chirality*. Whereas only two of the 18 Platonic and Archimedean polyhedral nets are (geometrically) chiral, *all* toroidal entanglements are likely to be (topologically) chiral [13]!

4.3. Free tilings

Before moving to hyperbolic space, we introduce an enlarged class of tilings, beyond those considered by Dress *et al.* [1,2]. The broader class includes examples whose orbifolds have finite area, but whose tiles are no longer finite. We call these cases *free tilings*. A formal extension of combinatorial tiling theory to include free tilings is in progress. Given the finite nature of S^2 , free tilings cannot form in that space; they can however, be realized in E^2 and H^2 .

The symmetry groups of E^2 that admit free tilings within the Coxeter, hat and stellate classes of orbifolds are $*2222$, 2222 , $2*22$ and $22*$. Consider the simplest example of a free tiling, made of ribbons bounded by

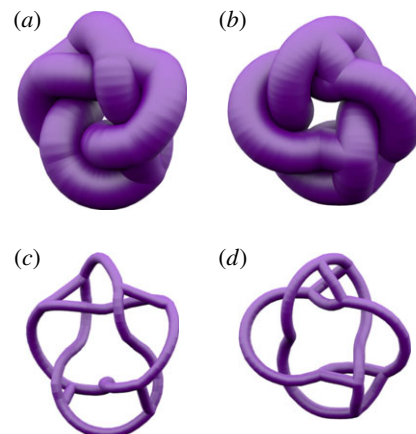


Figure 7. Tight embeddings of toroidal cube isotopes, found by the adapted SONO algorithm, which minimizes the total edge length in E^3 for unit diameter (non-overlapping) edges. (a) The tight embedding of the embedded graph shown in figure 3 whose skeleton is illustrated in (c). (b, d) Tight embedding and the edge skeleton of the toroidal isotope illustrated in figure 5.

parallel straight edges ($*2222$). Define two lattice vectors within the free tiling that define a single (or pair) of gluings to form cylindrical (or toroidal) polyhedra in E^3 . The orientation of these vectors determines the pitch of the resulting cylindrical helices forming tile edges. The number of interwoven cylindrical helices is also flexible, and depends on the gluing vector (figure 8*c,e*). Similarly, gluing the cylinder to form a torus decorated by parallel lines typically results in woven three-dimensional patterns with multiple components (figure 8*d,f*).

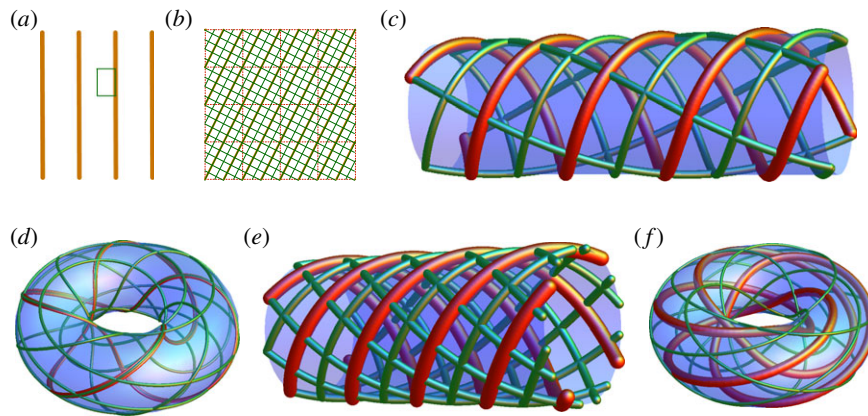


Figure 8. (a) A portion of a two-dimensional Euclidean free tiling (brown parallel lines), with an overlaid quadrilateral (in green) indicating a $*2222$ orbifold of the tiling. If glued along one of the pair of parallel edges formed by the larger red quadrilaterals in (b), the tiling covers the cylinder in a one-periodic double-helical pattern (c), which can be glued along the pairs of edges to produce a torus reticulated by a pair of interwoven loops (d). Alternatively, a different gluing pattern generates the triple-helical pattern of (e) which can be glued to produce the three-link pattern in (f).

Euclidean free tilings, though uninteresting in detail, illustrate a powerful aspect of our enumeration procedure: two-dimensional free tilings generally induce *multi-component interwoven* three-dimensional patterns.

5. TILINGS OF H^2

Two-dimensional hyperbolic space, H^2 , shares many of the features already encountered in the other homogeneous two-dimensional spaces: flat (E^2) and elliptic (S^2). Its intrinsic structure, however, allows a far greater wealth of structural types than in the other more familiar spaces. In turn, we find that mapping symmetric hyperbolic tilings with low flag transitivity into E^3 leads to a rich vein of highly symmetric Euclidean infinite polyhedra, whose edges form three-periodic (crystalline) nets, and intricate three-dimensional weavings.

We represent the geometry of H^2 using a model discovered by Poincaré that maps the entire space into the unit disc in such a way that angles between hyperbolic space lines are preserved. Lengths, however, are significantly distorted, so that regular patterns in H^2 may appear less so in the Poincaré disc. For example, H^2 can be tiled with identical geodesic triangular tiles whose vertices have angles $\pi/2, \pi/4, \pi/6$, illustrated in figure 9. Geodesics (straight lines) in H^2 map to circular arcs that meet the boundary of the disc orthogonally in the model. If we ignore colour, the triangle edges are mirror lines and the pattern forms from the Coxeter orbifold $*246$. (The coloured pattern requires the stellate orbifold 246.)

In contrast to the other two-dimensional elliptic and Euclidean spaces that sit comfortably within E^3 , any embedding of H^2 is necessarily frustrated. For example, the triangular tiling shown in figure 9 illustrates one possible embedding, that is evidently heavily distorted, since the triangles are increasingly diminished away from the disc centre. Hilbert proved that H^2 cannot be embedded in E^3 as a surface with constant negative curvature without singularities. An example that does indeed contain a singular edge, is the pseudosphere, described historically in Stillwell [14]. An alternative

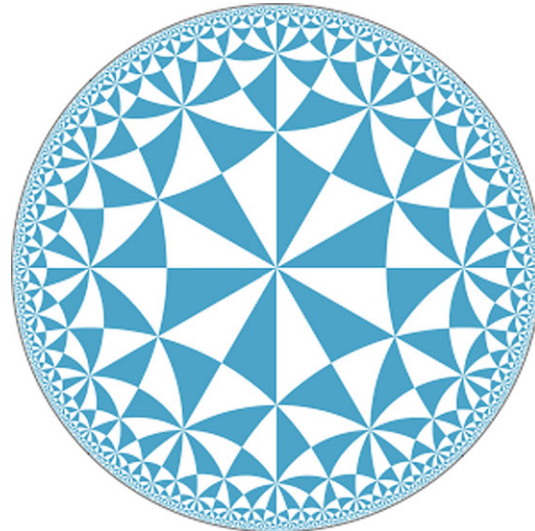


Figure 9. Representation of H^2 in the Poincaré disc model, tiled here with identical right triangles, whose vertices have angles of $\pi/2, \pi/4, \pi/6$. The apparent shrinkage of the tiles with increasing distance from the centre is an artefact of the model; all tiles are identical in H^2 .

way to embed H^2 within E^3 , that avoids cusps, is to wrap it onto a finite or a periodic surface, introducing local curvature variations. This approach is analogous to the maps from E^2 onto the torus and cylinder.

We look for embeddings that induce symmetric curvature variations that are as small as possible. Just as in the Euclidean case, we restrict attention to discrete groups of isometries that have a subgroup of translations. There are only 17 of these in E^2 , but infinitely many hyperbolic crystallographic groups. These are described by their orbifold symbol, and can be ranked by their hyperbolic area. The smallest-area hyperbolic orbifold (and the most symmetric discrete group in H^2) is $*237$. No embedding into E^3 is known that conserves this symmetry; an unsurprising result given the incompatibility of order-seven isometries with extended three-dimensional space. The most symmetric known embedding of H^2 in E^3 is based on the $*246$ orbifold. This is the intrinsic

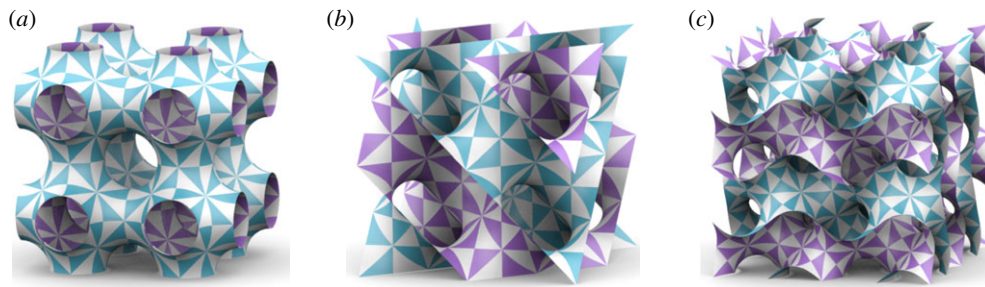


Figure 10. Embedded TPMS with two-dimensional symmetries $*246$. Asymmetric triangular domains corresponding to single orbifolds are alternately coloured and uncoloured. (a) The P surface. (b) The D surface. (c) The $Gyroid$.

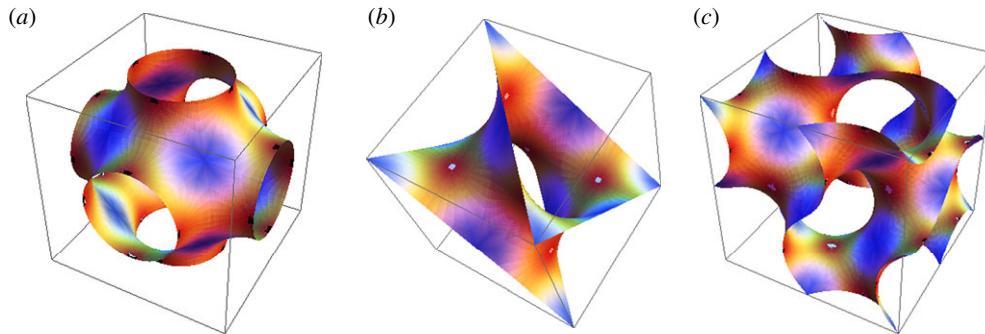


Figure 11. Conventional unit cells of TPMS coloured according to their curvature (flat points are blue, more negatively curved domains are red.) (a) The P surface, (b) the D surface and (c) the $Gyroid$ (cf. figure 4).

symmetry of the P , D and $Gyroid$ three-periodic minimal surfaces (TPMS). All three TPMS are shown in figure 10. (Some two-dimensional symmetries of the $Gyroid$ do not lift to three-dimensional isometries of E^3 , so that the asymmetric domain of this embedding in E^3 consists of a pair of $*246$ orbifolds, corresponding to the stellate 246 orbifold.)

Notice that all $\pi/2, \pi/4, \pi/6$ triangles are now equal in the P and D surfaces and that there are two distinct triangles in the $Gyroid$. The ‘coarse-graining’ of H^2 with this symmetry leads to embeddings with no loss of integrity at this resolution, when embedded in E^3 , though curvature distortions of H^2 occur within the triangular patches corresponding to single $*246$ domains, as shown in figure 11. (Other TPMS offer useful, though more distorted, embeddings of H^2 into E^3 .)

5.1. Crystalline three-dimensional nets from H^2

The map from H^2 into E^3 using TPMS is reminiscent of that from E^2 onto a cylinder, discussed in §4. Recall that in the latter case, one of the pair of lattice vectors in a two-periodic planar pattern becomes a gluing vector defining the equator of the cylinder, while the other remains free, resulting in a one-periodic cylinder reticulation (figure 2*b,c*).

In the two-dimensional hyperbolic case, patterns with $*246$ symmetry contain an unlimited number of translational subgroups. There is one particular translational subgroup generated by six independent translations that permits a $*246$ -preserving embedding onto all three of the P , D and $Gyroid$ surfaces [15]. For each surface, three hyperbolic translations map to the three independent direction vectors of E^3 , and the other three independent hyperbolic translations

Table 2. Regular hyperbolic nets formed from flag-transitive tilings of H^2 mapped onto the P , D or $Gyroid$ surfaces, with Schläfli symbol $\{n, z\}$.

$\{n, z\}$	surface	net name (<i>Epinet</i> [17] and RCSR [18])
$\{4, 6\}$	P	<i>sqc1</i> pcu
	D	<i>sqc947</i> hxg
	G	<i>sqc4991</i> bcs
$\{6, 4\}$	P	<i>sqc970</i> sod
	D	<i>sqc35</i> nbo
	G	<i>sqc5579</i> lcs
$\{6, 6\}$	P	<i>sqc947</i> hxg
	D	<i>sqc889</i> crs
	G	<i>sqc1</i> pcu

become ‘gluings’. The choice of which hyperbolic translations become gluings versus Euclidean translations is somewhat flexible; hence the three globally distinct embeddings (figure 10) for a single hyperbolic pattern. Embeddings of $*246$ onto other (two- or three-periodic) surfaces are possible, but are less homogenous and are not considered further here.

Given a symmetry group ($*246$) and a placement of the surface in space, we look for hyperbolic patterns (tilings) whose symmetries are a subgroup of $*246$ and a supergroup of these translations. This constraint is arbitrary, and has been imposed to limit the enumeration to a manageable process, determined by combinatorial tiling theory. The hyperbolic tilings are mapped onto the TPMS; resulting polygonal faces and edges on the TPMS form infinite polyhedra. Just three of these map to plane-faced regular infinite polyhedra, discovered

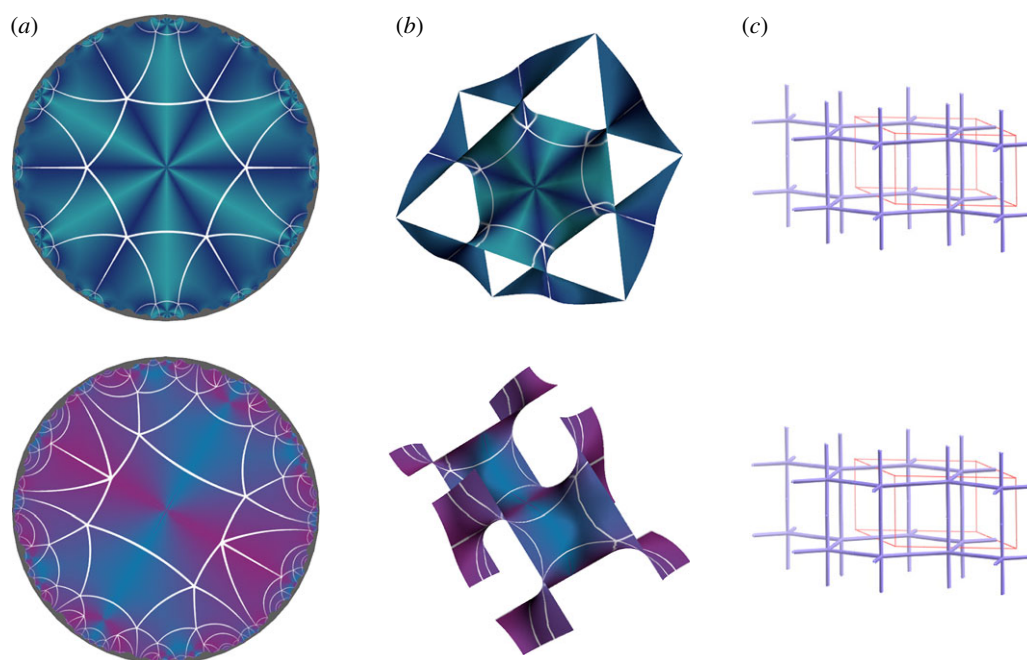


Figure 12. (a) Distinct hyperbolic tilings, of different orbifolds ($*2626$ and $*2^6$), (b) mapped onto different TPMS (P and D) generate the same s-net ((c) $sqc12$).

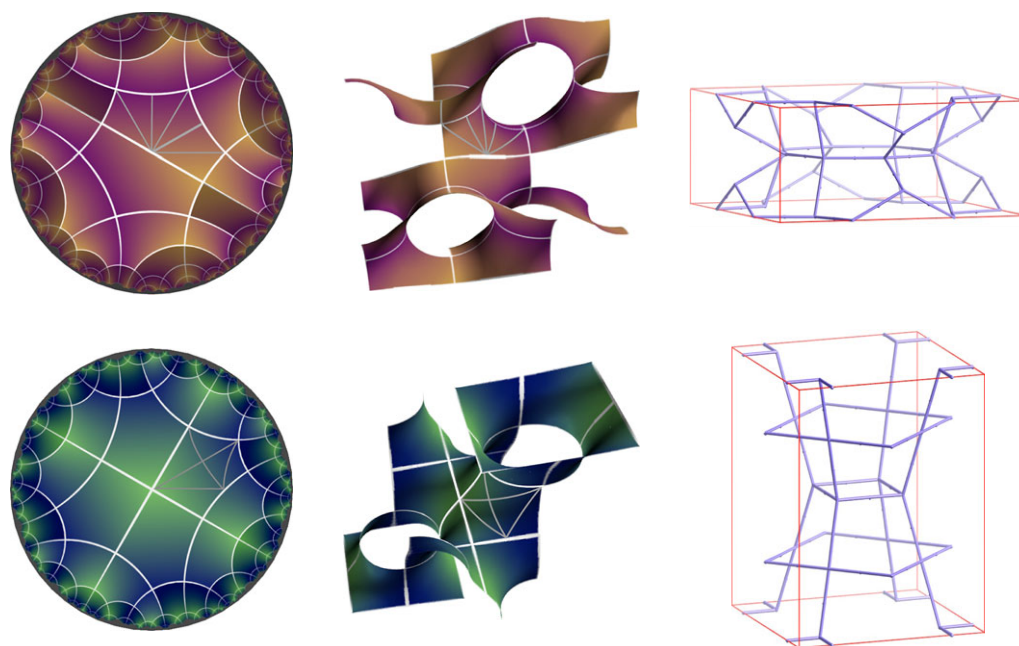


Figure 13. A pair of equivariant hyperbolic tilings, sharing orbifold $*2224$ but occurring in different subgroups on the P , leading to distinct nets.

somewhat remarkably in the twentieth century by English schoolboys, 2000 years after Plato [16]! As for the regular polyhedra in S^2 , we search for $\{p,q\}$ tilings with just one flag, generated via $*2pq$ (equivalent to $*2qp$) orbifolds. The plane-faced examples are flattened versions of the generic infinite polyhedra with symmetries $*246$ ($\{4,6\}$ and $\{6,4\}$ on the P surface), and $*266$ ($\{6,6\}$ on the D surface); analogous to the Platonic polyhedra as flattened spherical tilings.

However, further examples are regular two-dimensional tilings of three-periodic hyperbolic surfaces, and are realized in three-dimensional space

as flag-transitive tilings. We find the additional regular polyhedra (with non-planar faces) corresponding to $\{4,6\}$ and $\{6,4\}$ on the *Gyroid*, $\{6,6\}$ on the P and *Gyroid* and $\{4,6\}$ and $\{6,4\}$ on the D surface. Our prime focus, however, is on the formation of infinite three-periodic embedded in E^3 , derived from edges and vertices of these polyhedra.

The resulting patterns provide a rich sample of three-periodic Euclidean nets. Nets derived from the extended family of infinite regular polyhedra on the P , D and *Gyroid* surfaces are listed in table 2. Nets can be classified as equivalent according to various criteria. We are

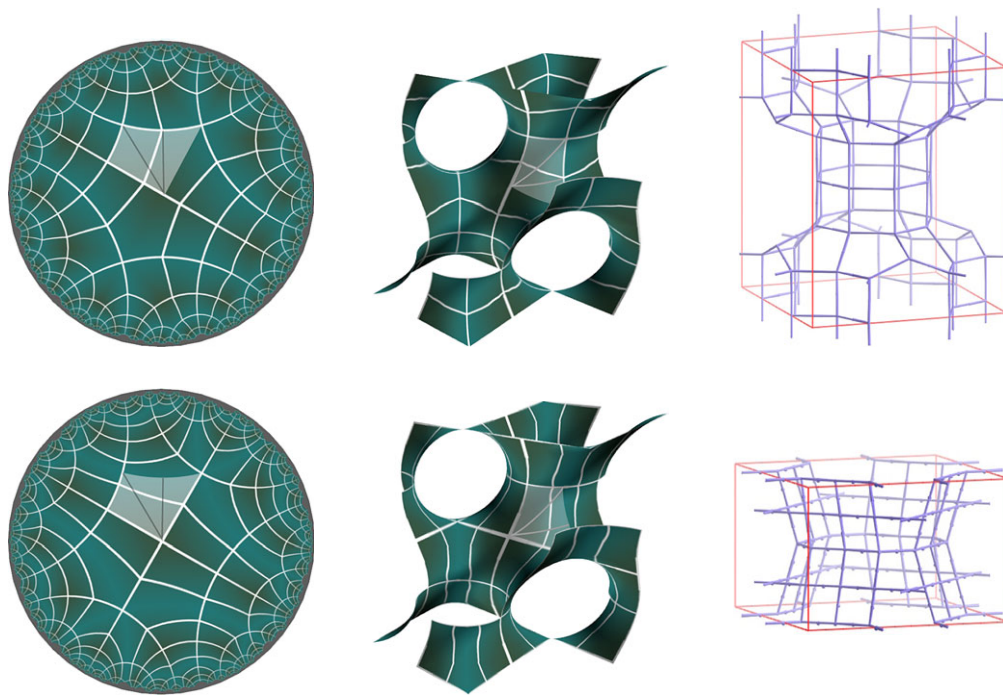


Figure 14. Mappings of the same hyperbolic tiling onto an identical domain of the P with different embeddings, forming distinct three-dimensional nets.

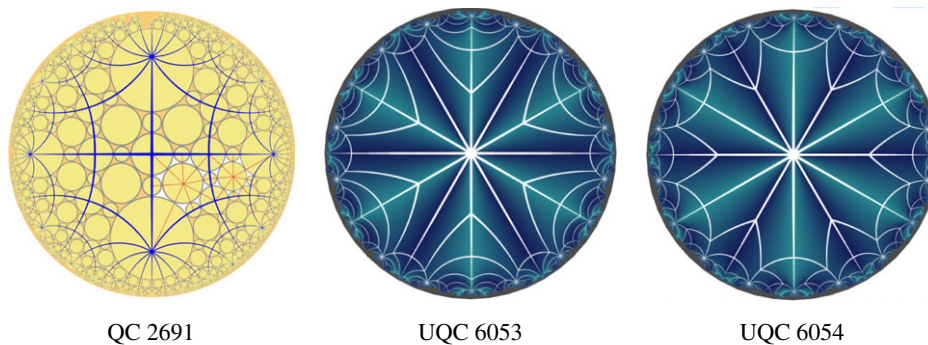


Figure 15. A $*2626$ tiling which generates two U-tilings related by transposition of the sixfold symmetry points, giving rise to the same pair of nets on the P and D , but distinct nets on the *Gyroid*.

interested in two distinct equivalence classes, according to their topology or isotopy, as discussed in §4.2.

Identification of topologically equivalent three-dimensional nets is possible using the concept of *equilibrium placement*, developed by Delgado-Friedrichs & O’Keeffe [19]. This offers a signature for topologically equivalent nets, and an effective canonical geometrical embedding of the net with maximal symmetry in E^3 . For example, this technique confirms the topological equivalence of the three-dimensional embeddings of multiple distinct two-dimensional hyperbolic tilings illustrated in figure 12. Likewise pairs of regular polyhedra listed in table 2 result in topologically equivalent nets, hence carry the same net names.

The regular infinite nets are the simplest examples of three-dimensional nets that emerge from systematic enumeration of tilings of H^2 that can be projected onto the simplest TPMS. Construction of those nets is a long-term project that continues; to date, the Coxeter tilings have been enumerated for all nets containing up

to two symmetrically distinct vertex types per orbifold; stellates are now in progress. Results are extensively catalogued on-line in the *Epimet* database [17]. The group theory and geometry involved in forming these nets are described (in some detail for Coxeter orbifolds) elsewhere [20].

The technique has a number of subtleties, principally owing to the many-to-many character of the mapping of tilings from H^2 to nets in E^3 . This means that a single hyperbolic tiling can induce a number of topologically distinct three-periodic nets in E^3 . This variety emerges as a natural consequence of the multiple possible foldings of H^2 onto either distinct, or indeed the same compatible TPMS. Additional degrees of freedom in mapping a single tiling onto a given TPMS arise as follows. First, multiple subgroups of $*246$ can exist sharing the same orbifold, so that equivariant tilings in H^2 can form distinct nets when mapped onto a TPMS (figure 13). Second, the geometry of a TPMS may break symmetries present in a given hyperbolic tiling

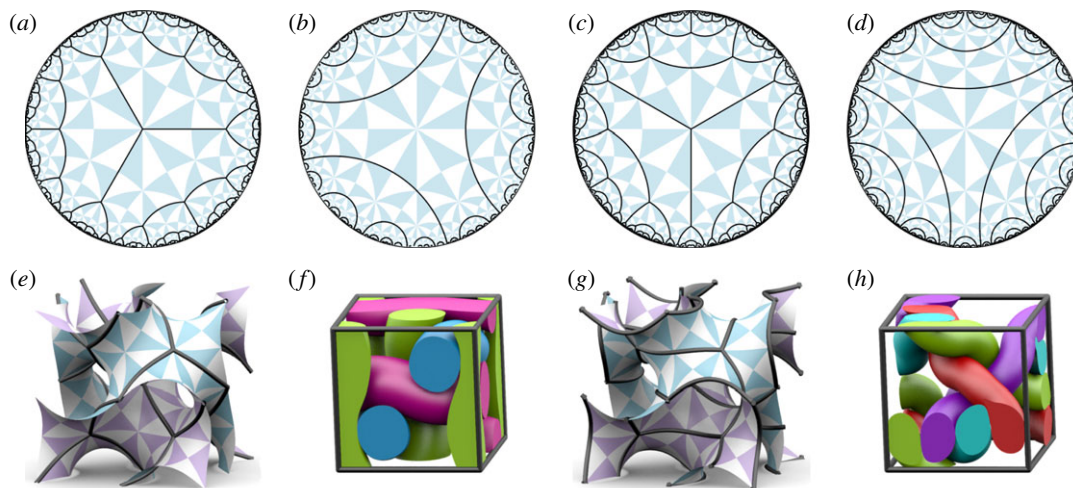


Figure 16. (a,b) Regular free tilings with symmetry $*2223$ containing (a) ribbon tiles and (b) branched ribbons. (c,d) Regular ribbon and branched ribbon tilings with symmetry $2*23$. (e,g) Embedding in E^3 of the regular ribbon tilings (a,c) via the *Gyroid*. (f,h) Embedding in E^3 of the branched ribbon tilings (b,d) via the *Gyroid*, giving helical packings, shown in their tight configurations.

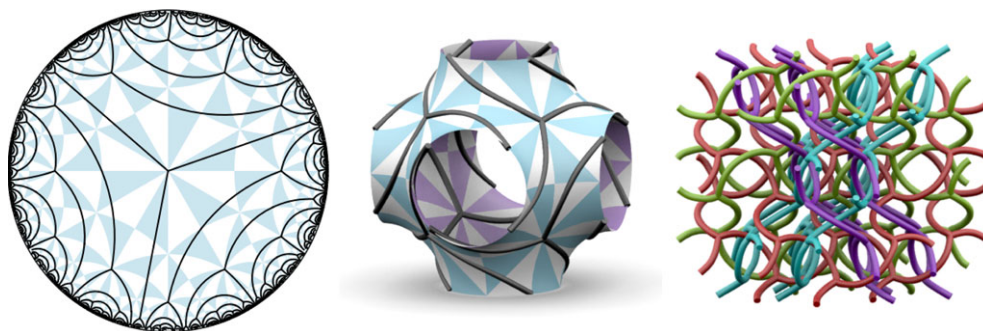


Figure 17. A regular ribbon tiling with symmetry 2223 , embedded into E^3 via the *P* surface, forming the inclined catenation [24] of **hcb** nets in four distinct orientations, and significantly interwoven.

leading to distinct embeddings of the same tiling within each TPMS (figure 14). Third, two distinct embeddings into E^3 via decorations of the *Gyroid* emerge when the two-dimensional tiling contains no mirror lines [21] (figure 15).

The multiplicity of three-dimensional nets from a single two-dimensional hyperbolic tiling is a fruitful feature of this approach to net enumeration. The situation is further complicated by the possibility of distinct two-dimensional tilings leading to equivalent three-dimensional nets, as for two of the nets listed in table 2.

We have shown above that distinct isotopes of toroidal nets can be constructed from different tilings of E^2 . Similarly, distinct entanglements of topologically equivalent three-periodic nets can be formed from various tilings of H^2 . The SONO algorithm, introduced in §4.2 offers a route to form a canonical geometry for net isotopes. Examples can be found in the next section.

5.2. Free tilings of H^2

Free tilings of H^2 offer a far richer variety of patterns than their cousins that inhabit E^2 (and related cylindrical and toroidal patterns), owing to the existence of multiple parallel geodesics in hyperbolic space. The Euclidean case allows free tilings of ribbon-shaped tiles; hyperbolic examples include ribbon and

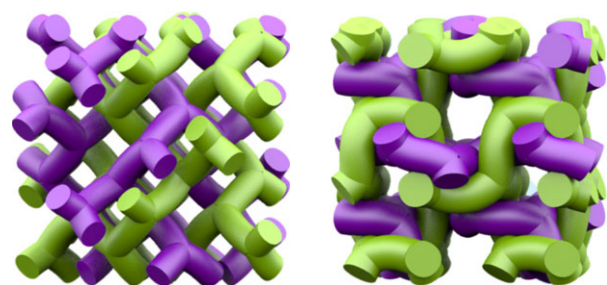


Figure 18. Tight embeddings of the interwoven nets formed from the free tilings on the *Gyroid* illustrated in figure 16e,g. Both examples are pairs of twofold interpenetrated (like-handed) **srs** nets; distinct tight embeddings are due to differences in the mutual **srs** entanglements.

branched-ribbon tiles, or combinations thereof [10]. Hyperbolic ‘ribbon’ and ‘branched ribbon’ tiles may have boundary morphologies that are tree-shaped or infinite geodesic lines. Ribbon-shaped tiles have exactly two boundary edges (either both tree-shapes or a combination of a tree and a line), and branched-ribbons are bounded by an infinite number of either hyperparallel lines, trees or a combination of the two. Free ribbon tilings have been referred to elsewhere as ‘close packed’ structures in H^2 [22]. Figure 16a–d illustrates

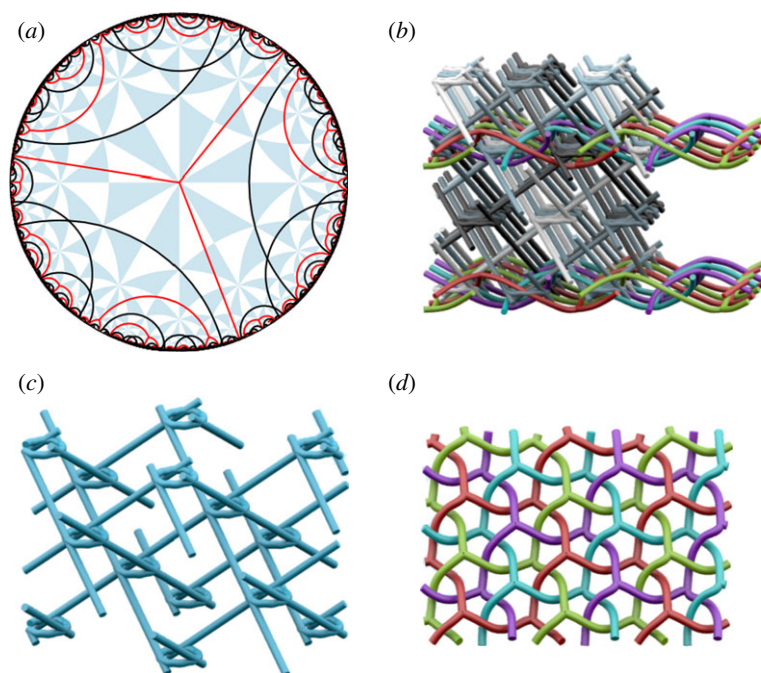


Figure 19. (a) A free tiling of H^2 composed of two distinct tree boundaries (full and broken). (b) Embedding of the tiling via the D surface gives four intergrown 3-periodic nets, which have no barycentric embedding owing to vertex collisions and are thus unidentified, interwoven with layers of four 2-periodic **hcb** nets. (c) View of one of the three-periodic nets and (d) the **hcb** weaving.

some examples that are ‘regular’ (one type of tile, edge and vertex).

Hyperbolic free tilings embed in E^3 to form arrays of nets or filaments, and combinations thereof, depending on the combination of boundary morphologies present in the original free tiling. Figure 16*e–h* shows some particularly interesting embeddings of free tilings via the *Gyroid*, some consisting of multiple three-periodic nets, and others solely of filaments. Two examples of free tilings that contain only branched ribbons with geodesic tile boundaries are shown, and both of these form (via the *Gyroid* and periodic SONO algorithm) canonical tight embeddings in E^3 that are arrays of mutually inclined helical filaments, figure 16*f,h*. When these filaments are straightened (isotopically), the arrays form crystallographic rod packings [23]. Other free tilings with branched ribbons and geodesic boundaries give three-dimensional arrays of interwoven loops, forming three-dimensional ‘chain-mail’ structures.

Free tilings whose tile boundaries are tree-shaped lead to a variety of embeddings in E^3 . Since the tile boundaries are branched, the resulting E^3 embeddings are also branched, giving finite, two-periodic or three-periodic net components, interwoven in a three-periodic pattern [10]. Regular ribbon tilings must embed in E^3 with symmetrically equivalent vertices and edges. For example, embeddings of regular ribbon tilings whose edges form degree-3 trees can have one of three possible geometries: the θ -graph (finite, with a pair of degree-three vertices), the two-periodic hexagonal net **hcb** [20] and three-periodic **srs** net. All have been found as embeddings of free tilings: an **hcb** example is shown in figure 17.

Both free tilings illustrated in figure 16*a,c* embed in E^3 as a pair of interwoven **srs** nets, figure 16*e,g*. This intergrowth has been classified as ‘twofold interpenetrated’ [24]; however, their entanglements differ,

clearly demonstrated by their distinct tight embeddings, determined using the SONO algorithm (figure 18). An alternative approach to distinguish net intergrowth modes is possible via the numerical *TOPOS* algorithm, developed by Blatov *et al.* [25], which determines explicit measures of entanglement of distinct cycles within intergrown nets. *TOPOS* confirms the distinct entanglements of **srs** nets in figure 16*e,g*: one contains 18 Hopf links and one more complex link; the other has 23 Hopf links and three more complex links.

Evidently, embeddings in E^3 of hyperbolic free tilings offer a variety of structural classes, as well as entanglements. Numerous less regular examples can be systematically enumerated using an extension to standard combinatorial tiling theory. These examples include combinations of tile types (ribbons or branched ribbons) as well as tile boundaries that are distinct in topology or a mix of tree-shapes and geodesics. The corresponding structures in E^3 contain the interweaving of distinct species of nets and filaments. For example, figure 19 shows a free tiling with two distinct tree-shapes as tile boundaries which maps via the D surface to a structure in E^3 that has three-periodic and two-periodic nets interwoven with one another.

6. CLOSING

This sketch of three-dimensional nets via two-dimensional tilings offers an indication of the variety of net types that emerge from the simplest possible tilings of the two-dimensional homogeneous spaces. In particular, it is clear that H^2 is sufficiently complex to furnish a wealth of examples whose systematic enumeration within the confines of three-dimensional space is difficult.

We do not claim exhaustive enumerations of three-dimensional patterns. Rather, accessing three-dimensional flat space (E^3) via tilings of the sphere, the torus and TPMS, which are generated by enumeration of tilings of their covering spaces, S^2 , \tilde{E}^2 and H^2 , affords a useful sample of three-dimensional nets, from the simplest examples related to Platonic polyhedra, to multiple interwoven nets and tangled net isotopes.

In our view, possibly the most striking aspect of the approach is the extraordinary relevance of very symmetric two-dimensional patterns to structurally useful patterns of some importance in E^3 [26]. For example, two of the most common nets encountered in structural chemistry, **hcb** and **srs**, result from the simplest (hyperbolic 2D) regular tree. A survey of nets encountered in metal-organic frameworks ('MOFs') noted 'that in the largest categories, those of triangular, tetrahedral, square, and octahedral geometries, the dominant nets are four out of the five regular nets, namely, **srs**, **dia**, **nbo**, and **pcu**' [27]. Platonic degree-3, -4 and -6 trees map via TPMS to three of these nets (**srs**, **dia** and **pcu**). Further, **nbo** forms via the D surface from the regular {6,4} tiling, while **pcu** is its two-dimensional dual, namely {4,6} (projected via the P surface). Both of the latter nets have orbifold symmetry $*246$, the most symmetric two-dimensional hyperbolic symmetry commensurate with three-dimensional space. A more recent collation ranks **dia**, **pcu**, **srs** and **ths** as the most prevalent nets in this class of materials [28]. A hyperbolic description of **ths** remains unknown.

Clearly, our task remains unfinished. Nevertheless, we are confident that this approach does afford a powerful route to enumeration of nets, both tangled and intergrown.

REFERENCES

- Dress, A. W. M. 1987 Presentations of discrete groups, acting on simply connected manifolds. *Adv. Math.* **63**, 196–212. (doi:10.1016/0001-8708(87)90053-3)
- Huson, D. H. 1993 The generation and classification of tile- k -transitive tilings of the Euclidean plane, the sphere, and the hyperbolic plane. *Geometriae Dedicata* **47**, 269–296. (doi:10.1007/BF01263661)
- Delgado-Friedrichs, O. 2003 Data structures and algorithms for tilings I. *Theoret. Comput. Sci.* **303**, 431–445. (doi:10.1016/S0304-3975(02)00500-5)
- Plato. *Timaeus*. ca. 360 BCE. See <http://classics.mit.edu/Plato/timaeus.html>.
- Conway, J. H. & Huson, D. H. 2002 The orbifold notation for two-dimensional groups. *Struct. Chem.* **13**, 247–256. (doi:10.1023/A:1015851621002)
- Conway, J. H., Burgiel, H. & Goodman-Strauss, C. (eds) 2008 *The symmetries of things*. Wellesley, MA: AK Peters Ltd.
- Saito, R., Fujita, M., Dresselhaus, G. & Dresselhaus, M. S. 1992 Electronic structure of graphene tubules based on C_{60} . *Phys. Rev. B* **46**, 1804–1811. (doi:10.1103/PhysRevB.46.1804)
- Kauffman, L. H. 1989 Invariants of graphs in three-space. *Trans. Am. Math. Soc.* **311**, 697–710. (doi:10.1090/S0002-9947-1989-0946218-0)
- Pieranski, P. 1998 In search of ideal knots. In *Ideal knots, Series on knots and everything*, vol. 19 (eds A. Stasiak, V. Katritch, L. H. Kauffman), pp. 20–41. Singapore: World Scientific.
- Evans, M. E. 2011 Three-dimensional entanglement: knots, knits and nets. PhD thesis, Australian National University, Acton, Australia.
- Castle, T., Robins, V. & Hyde, S. T. In preparation. Toroidal entangled polyhedral graphs: tetrahedra, octahedra and cubes.
- Hyde, S. T. & Schröder-Turk, G. 2007 Tangled (up in) cubes. *Acta Cryst. A* **63**, 186–197. (doi:10.1107/S0108767306052421)
- Castle, T., Evans, M. E. & Hyde, S. T. 2009 All toroidal embeddings of polyhedral graphs in 3-space are chiral. *New J. Chem.* **33**, 2107–2113. (doi:10.1039/b907338h)
- Stillwell, J. 1996 *Sources of hyperbolic geometry*. History of mathematics. Providence, RI: American Mathematical Society.
- Sadoc, J.-F. & Charvolin, J. 1989 Infinite periodic minimal surfaces and their crystallography in the hyperbolic plane. *Acta Cryst. A* **45**, 10–20. (doi:10.1107/S0108767388008438)
- Coxeter, H. S. M. 1937 Regular skew polyhedra in three and four dimensions. *Proc. Lond. Math. Soc.* **43**, 33–62. (doi:10.1112/plms/s2-43.1.33)
- Hyde, S., Robins, V. & Ramsden, S. 2008 Epinet. See <http://epinet.anu.edu.au>.
- O'Keeffe, M., Peskov, M. A., Ramsden, S. J. & Yaghi, O. M. 2008 The reticular chemistry structure resource (RCSR) database of, and symbols for crystal nets. *Acc. Chem. Res.* **41**, 1782–1789.
- Delgado-Friedrichs, O. & O'Keeffe, M. 2003 Identification of and symmetry computation for crystal nets. *Acta Cryst. A* **59**, 351–360. (doi:10.1107/S0108767303012017)
- Ramsden, S. J., Robins, V. & Hyde, S. T. 2009 Three-dimensional Euclidean nets from two-dimensional hyperbolic tilings: kaleidoscopic examples. *Acta Cryst. A* **65**, 81–108. (doi:10.1107/S0108767308040592)
- Robins, V., Ramsden, S. & Hyde, S. T. 2005 A note on the two symmetry-preserving covering maps of the gyroid minimal surface. *Eur. Phys. J. B* **48**, 107–111. (doi:10.1140/epjb/e2005-00377-x)
- Hyde, S. T. & Oguey, C. 2000 From 2d hyperbolic forests to 3d Euclidean entangled thickets. *Eur. Phys. J. B* **16**, 613–630. (doi:10.1007/PL00011063)
- O'Keeffe, M. & Hyde, B. G. 1996 *Crystal structures I. Patterns and symmetry*. Washington, DC: Mineralogical Society of America.
- Carlucci, L., Ciani, G. & Proserpio, D. M. 2003 Polycatenation, polythreading and polyknitting in coordination network chemistry. *Coord. Chem. Rev.* **246**, 247–289. (doi:10.1016/S0010-8545(03)00126-7)
- Blatov, V. A. 2006 Multipurpose crystallochemical analysis with the program package TOPOS. *IUCr CompComm. Newsl.* **7**, 4–38.
- Hyde, S. T., Delgado-Friedrichs, O., Ramsden, S. J. & Robins, V. 2006 Towards enumeration of crystalline frameworks: the 2d hyperbolic approach. *Solid State Sci.* **8**, 740–752. (doi:10.1016/j.solidstatesciences.2006.04.001)
- Ockwig, N. W., Delgado-Friedrichs, O., O'Keeffe, M. & Yaghi, O. M. 2005 Reticular chemistry: occurrence and taxonomy of nets and grammar for the design of frameworks. *Acc. Chem. Res.* **38**, 176–182. (doi:10.1021/ar0200221)
- Alexandrov, E. V., Blatov, V. A., Kochetkova, A. V. & Proserpio, D. M. 2011 Underlying nets in three-periodic coordination polymers: topology, taxonomy and prediction from a computer-aided analysis of the Cambridge structural database. *Cryst. Eng. Commun.* **13**, 3947–3958. (doi:10.1039/C0CE00636J).